

Article

Analysis and Design of Wireless Power Transfer System for Rotational Inertial Navigation Application

Meng Niu ¹, Xinglin Sun ^{1,*}, Hongyu Ma ², Zhijuan Zhu ³, Tiantian Huang ¹ and Kaichen Song ²

¹ College of Biomedical Engineering and Instrument Science, Zhejiang University, Hangzhou 310027, China; niu@zju.edu.cn (M.N.); tthuang@zju.edu.cn (T.H.)

² School of Aeronautics and Astronautics, Zhejiang University, Hangzhou 310027, China; 3170101710@zju.edu.cn (H.M.); kcsong@zju.edu.cn (K.S.)

³ Advanced Technology Institute, Zhejiang University, Hangzhou 310027, China; zjzhu@zju.edu.cn

* Correspondence: xlsun@zju.edu.cn

Abstract: Cables or slip-rings are often used to power loads on a rotating unit in the rotation modulated inertial navigation system (RMINS). However, these power supply methods have the disadvantages of cable winding and slip ring friction and wear, which reduces the reliability and life of the RMINS. Therefore, this paper applies magnetic coupling resonant wireless power transfer (MCRWPT) technology to the RMINS to avoid the shortcomings of the above power supply methods. Furthermore, according to the structure and working characteristics of the RMINS, a simple design method of the MCRWPT system without any feedback control is proposed. Based on the ANSYS simulation, the magnetic shielding structure is designed to reduce magnetic leakage, and the efficiency of the MCRWPT system is optimized by designing the excitation frequency. Experiments verify the effectiveness of the proposed method. The experimental results show that the designed MCRWPT system can achieve an efficiency of 74.6% with an output power of 10 W and has been successfully applied to the uniaxial rotation module inertial navigation system. Finally, the design method of the MCRWPT system is simple, and it has guiding significance for the design of the wireless power transfer system in the RMINS.

Keywords: wireless power transfer; magnetic coupling resonant; excitation frequency; rotation modulated; inertial navigation system



Citation: Niu, M.; Sun, X.; Ma, H.; Zhu, Z.; Huang, T.; Song, K. Analysis and Design of Wireless Power Transfer System for Rotational Inertial Navigation Application. *Appl. Sci.* **2022**, *12*, 6392. <https://doi.org/10.3390/app12136392>

Academic Editor: Eun S. Lee

Received: 18 May 2022

Accepted: 22 June 2022

Published: 23 June 2022

Publisher's Note: MDPI stays neutral with regard to jurisdictional claims in published maps and institutional affiliations.



Copyright: © 2022 by the authors. Licensee MDPI, Basel, Switzerland. This article is an open access article distributed under the terms and conditions of the Creative Commons Attribution (CC BY) license (<https://creativecommons.org/licenses/by/4.0/>).

1. Introduction

Rotation modulation technology is an effective method to improve the accuracy of inertial navigation systems (INSs) at a low cost [1]. This technology can suppress constant or slow variation errors of inertial devices by rotating the inertial measurement unit (IMU) continuously or periodically [2]. Therefore, the power supply to the rotating part is a key technology. If the rotation scheme is set to continuous rotation or run-stop in forward and reverse directions, winding reels can be used to transmit electrical energy from the stationary unit to the rotating unit. However, wired electrical energy transfer can damage safety under loss of indexer control and restrict the free rotation of rotating parts in the rotation modulated inertial navigation system (RMINS). Therefore, applying slip-rings to solve the cable winding problem is a common method for the power supply of rotating units [3]. Nevertheless, slip-rings have the drawbacks of wear and friction, limited lifetime, and regular maintenance [4]. Based on these problems, applying wireless power transfer (WPT) technology to the RMINS is necessary to power the rotating units through a non-contact method.

Electronic circuits or sensors are often installed on the rotating part in practical applications, such as shaft torque measurement [5], north finder [6], and the RMINS. The application of WPT can obviate the shortcomings of wires, wire reels, and slip-rings and greatly improve the reliability and lifetime of the system. Despite the great advantages, the

WPT system also has some disadvantages. The performance of nearby electrical circuits was influenced by the electromagnetic interference noise produced by a WPT system [7]. For rotary equipment such as the RMINS, where sensors and circuits are installed on the rotating part with limited space, the magnetic flux leakage of WPT can adversely affect sensors and circuits [8]. The magnetic sensitivity index restriction of interferometric fiber optic gyroscope used in typical INSs is $0.0001\text{--}0.001^\circ\text{h}^{-1}\text{G}^{-1}\text{s}^{-1}$ [9]. Therefore, it is necessary to design a magnetic shielding structure to reduce the magnetic field leakage of the WPT system. Moreover, the limited space of the rotating part restricts the size of the receiving circuit and the winding topology for a WPT system. Therefore, the mature products of the WPT system are unsuitable for direct application in the RMINS [10].

Nowadays, electromagnetic induction wireless power transfer (EMIWPT) is often used for short-range WPT. However, a gap between the primary and secondary coil reduces the efficiency of EMIWPT. Compared with the EMIWPT, the magnetic coupling resonant wireless power transfer (MCRWPT) achieved higher power transmission efficiency (PTE) at a longer distance between the two coils [11]. Therefore, to improve the PTE of the system, the MCRWPT used in the rotary equipment is suitable because the gap exists between the primary coil and secondary coil.

In recent years, several further efforts have been dedicated to applying the MCRWPT system. The related researchers have studied the MCRWPT system from two main aspects to reduce magnetic leakage and improve PTE. On the one hand, the winding topology of WPT was studied, such as optimizing coil structure and designing magnetic shield structure [12]. A novel double-layer parallel coil model was proposed for the rotary equipment to improve the PTE and output power, and the performance of the WPT system was better than that of a conventional single-layer coil [13]. However, the application of WPT caused magnetic field leakage, which adversely affected surrounding materials and humans [14]. Thus, different methods such as passive shielding, active shielding, and eliminating the magnetic field with a reactive resonant current loop were introduced to suppress magnetic field leakage [15]. To further reduce magnetic leakage, optimizing the geometry of the winding was given, which reduced the magnitude of the near magnetic field by 29.12% [16]. However, the above methods are mainly applied to electric vehicles, and there are few research methods to reduce magnetic flux leakage in rotary equipment. For a pot core rotating transformer, the different winding topologies in the rotating transformer were designed and optimized according to total core volume and power losses [17]. Furthermore, a multi-physical design method for high-frequency rotating transformers was proposed, where the PTE was optimized for different core geometries [18]. The design of the rotary transformer is mainly based on the combination of multiple physical fields, such as electric field, magnetic field, and thermal field, which increases the complexity of system design.

On the other hand, compensation topology was researched for performance improvement. The capacitor compensation schemes of MCRWPT mainly included four categories, namely series-series (SS), series-parallel, parallel-series, and parallel-parallel, and the characteristics of these schemes were analyzed [19]. The SS capacitor compensation scheme has the characteristic that resonance frequency is independent of load resistance and is more suitable for the variable load resistance on the rotating part. However, the output voltage of the WPT increases with increasing load resistance under the condition that the input voltage is constant. A direct current to direct current (DC-DC) boost-buck converter with a limited input voltage range was applied to adjust the output voltage of the rectifier [20,21]. The efficiency of the DC-DC converter was related to the load resistance, and its maximum efficiency was between 60% and 90% [22]. A closed-loop control scheme was applied to achieve the maximum efficiency under the non-optimal equivalent load resistance condition [23]. However, the application of the closed-loop control method introduced wireless communication into the MCRWPT system, which increased the complexity of the system. Some methods without wireless communication were proposed. Adjusting frequency and input voltage by monitoring input voltage and input current achieved system efficiency above 70% [24]. In addition, the maximum energy efficiency tracking method was achieved

by adjusting the equivalent load resistance inside the receiving unit to the optimal value and then finding the minimum input power in the transmitting unit [25]. However, this method requires a fixed system output power. In addition, the MCRWPT scheme with DC-DC converters needs closed-loop control, which makes the system design complex on the premise of improving the system performance. Most research focuses on applying WPT technology to electric vehicles and rotating shaft equipment. However, there are few types of research on the application of WPT technology in an RMINS.

To enhance the safety of the RMINS and improve the flexibility of the rotation control scheme, the WPT technology is introduced into the RMINS in this paper. Since the existing WPT system’s coil shape is matched to the circuit parameters, it cannot be directly applied to the limited size structure within the RMINS. This paper proposes a simple design method for the MCRWPT system applied in the RMINS. The magnetic shielding structure is designed to reduce magnetic leakage, and the excitation frequency is studied to improve the efficiency of the MCRWPT system with a DC-DC converter. This system can provide a stable power supply for the rotating unit without feedback control. Finally, the experiment verifies that MCRWPT technology can be successfully applied in the RMINS.

The structure of this paper is arranged as follows. The principle and characteristics of the MCRWPT system is analyzed in Section 2. The MCRWPT system is designed from two aspects of magnetic shielding structure and excitation frequency in Section 3. The experiment results are analyzed, and the prototype is given in Section 4. A brief conclusion is given in Section 5.

2. Analysis of MCRWPT System for RMINS

2.1. Principle of MCRWPT System

Equivalent circuit theory is applied to research the MCRWPT system based on the two-coil model with SS structure in this paper [26]. The equivalent circuit model is shown in Figure 1, where the U_S represents the alternating current power supply. The internal resistance R_S of the power supply and resistance of the transmitting coil constitute equivalent resistance R_1 of the transmitter. C_1 and L_1 represent the compensation capacitance and inductance of the transmitter, respectively. The compensation capacitance and inductance of the receiver are denoted by the symbols C_2 and L_2 , respectively. The symbol R_2 is the equivalent resistance of the receiver, and R_L is the equivalent load resistance. The mutual inductance between the transmitting and receiving winding is denoted as M . i_1 and i_2 are the transmitter and receiver currents, respectively. The relationship between the mutual inductance M and the coupling coefficient k is shown in Equation (5).

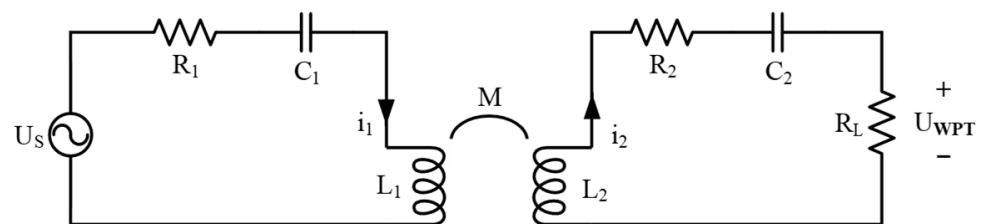


Figure 1. Equivalent circuit of the MCRWPT system.

According to Kirchhoff’s law, when the power source U_S outputs alternating voltage at the frequency of $f = \omega / (2\pi)$, the equivalent circuit equation under the sinusoidal steady state of the system is obtained by Equations (1) and (2).

$$Z_1 \cdot i_1 - j\omega M \cdot i_2 = U_S \tag{1}$$

$$Z_2 \cdot i_2 - j\omega M \cdot i_1 = 0 \tag{2}$$

$$Z_1 = R_1 + j\omega L_1 + \frac{1}{j\omega C_1} \tag{3}$$

$$Z_2 = R_2 + R_L + j\omega L_2 + \frac{1}{j\omega C_2} \tag{4}$$

$$M = k \cdot \sqrt{L_1 \cdot L_2} \tag{5}$$

The voltage gain G_V , output power P_{OUT} , and PTE η_{WPT} are derived from Equations (1)–(4):

$$G_V = \frac{\omega M R_L}{Z_1 \left(Z_2 + \frac{\omega^2 M^2}{Z_1} \right)} \tag{6}$$

$$P_{OUT} = \frac{\omega^2 M^2 R_L U_S^2}{\left(Z_1 + \frac{\omega^2 M^2}{Z_2} \right)^2 \left((R_2 + R_L)^2 + \left(\omega L_2 - \frac{1}{\omega C_2} \right)^2 \right)} \tag{7}$$

$$\eta_{WPT} = \frac{\omega^2 M^2 R_L}{Z_2^2 \left(Z_1 + \frac{\omega^2 M^2}{Z_2} \right)} \tag{8}$$

When the MCRWPT system works in the resonance state, there are:

$$\omega L_1 - \frac{1}{\omega C_1} = \omega L_2 - \frac{1}{\omega C_2} = 0 \tag{9}$$

Substituting Equations (3)–(5) in Equations (6) and (8) with the parameters listed in Table 1, the voltage gain and PTE as functions of equivalent load resistance, excitation frequency, and coupling coefficient are calculated. In Table 1, the coil inductance refers to the primary coil parameter of power transmitter design A10 that complies with the Qi wireless charging standard. When the input voltage U_S amplitude is set to 19 V, the output voltage U_{WPT} and PTE are plotted in Figure 2. The formula for calculating the output voltage is $U_{WPT} = G_V \cdot U_S$. Figure 2a shows that the amplitude of output voltage increases with the increase of the equivalent load resistance under the conditions that the excitation frequency is 100 kHz and the coupling coefficient is 0.8. It can be seen from Figure 2b that the output voltage increases first and then decreases with the increase of the excitation frequency under the conditions that R_L is 50 Ω and k is 0.8. The maximum output voltage occurs at the resonant frequency of 100 kHz. The variation trend of output voltage with coupling coefficient is shown in Figure 2c. In the resonant state, the output voltage increases first and then decreases with the increase of coupling coefficient. Therefore, the output voltage of MCRWPT is affected by the equivalent load resistance, excitation frequency, and coupling coefficient. If the R_L changes, the output voltage will not be stabilized at a constant value.

Table 1. Parameters used for calculations.

Parameters	Value	Unit
Transmitter resistance R_1	0.53	Ω
Receiver resistance R_2	0.23	Ω
Coil inductances L_1, L_2	24	μH
Compensation capacitors C_1, C_2	105.54	nF
Resonant frequency f	100	kHz

The PTE variation trend with the increasing equivalent load resistance is shown in Figure 2d. The resonance state has an equivalent load resistance to achieve maximum PTE. It can be seen from Figure 2e that the PTE increases first and then decreases with the excitation frequency under the conditions that $R_L = 50 \Omega$ and $k = 0.8$. The maximum PTE occurs at the resonant frequency of 100 kHz. Figure 2f shows that the PTE increases when the equivalent load resistance increases under the conditions that f is 100 kHz and k is 0.8. Therefore, increasing the PTE of the system can be achieved by increasing k , making the system work in a resonant state, and changing the equivalent load resistance.

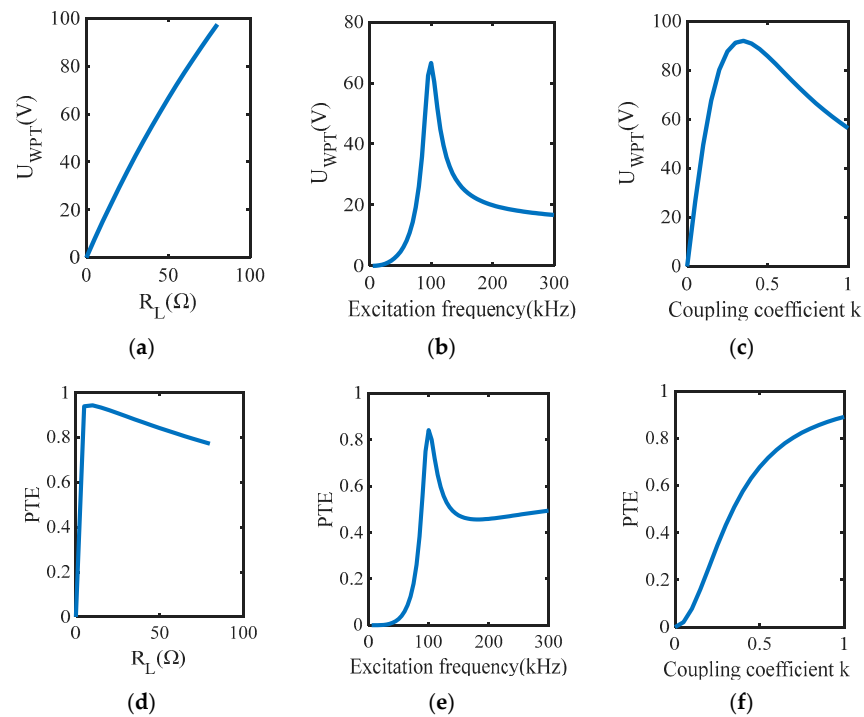


Figure 2. The relationship between output voltage, PTE and excitation frequency, equivalent load resistance, and coupling coefficient. (a) Output voltage changes with equivalent load resistance. (b) Output voltage changes with excitation frequency. (c) Output voltage changes with coupling coefficient. (d) PTE changes with equivalent load resistance. (e) PTE changes with excitation frequency. (f) PTE changes with coupling coefficient.

As shown in Figure 3, when the coupling coefficient is greater than 0.35, the output power decreases with the increase of the coupling coefficient under the conditions that R_L is 50 Ω and f is 100 kHz. Therefore, the design of the MCRWPT system needs to consider the influence of the coupling coefficient on output power in the case of constant input voltage.

The theoretical analysis shows that the output voltage and PTE of the MCRWPT system are affected by R_L , excitation frequency, and k when the primary and secondary coils' inductance, the resonant compensation capacitor of the primary and secondary coils, and the input voltage are constant. When MCRWPT is applied to the RMINS, depending on the internal structure in the RMINS, the power supply system can work properly and achieve higher PTE by selecting the appropriate excitation frequency for a given coil diameter and magnetic shielding structure.

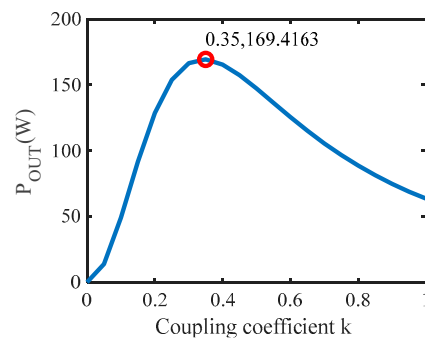


Figure 3. The relationship between output power and coupling coefficient.

2.2. Characteristics of MCRWPT for the RMINS

The MCRWPT system applied to power a single-axis RMINS is shown in Figure 4. The principle of the single-axis RMINS is that the motor drives the rotating unit to perform

periodic rotation to suppress the error from inertial sensors. The IMU mounted on the rotating unit is the load for the receiver of the MCRWPT system. The IMU consists of three gyroscopes, three accelerometers, and an information processing PCB, where the gyroscopes and accelerometers are mounted orthogonally. The transmitter and receiver form the MCRWPT system. Both the transmitter and receiver include corresponding PCBs and coils. The DC power supply powers the transmitter of the wireless power.

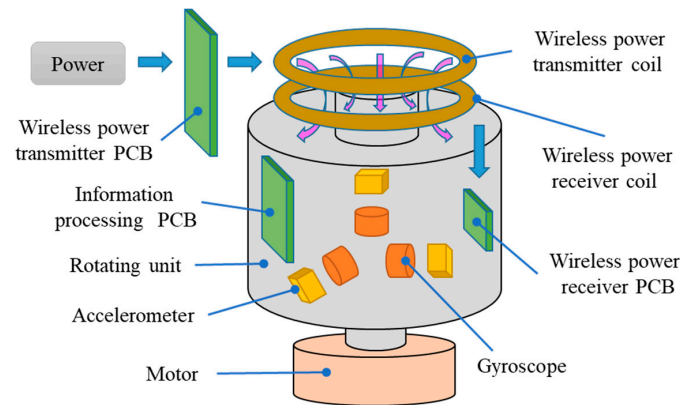


Figure 4. Arrangement of the components of the MCRWPT system for an RMINS.

According to the structure of the RMINS, the MCRWPT system needs to be designed and implemented with the following characteristics: First, the magnetic shielding structure is needed to reduce the leakage of the magnetic field because the inertial sensors and the framework are sensitive to the alternating magnetic field. Second, a suitable gap between the primary and secondary sides is needed due to the rotating unit's rotation. Third, the output voltage of the MCRWPT system is stable, and the output voltage ripple should be less than 50 mV. Otherwise, the accuracy of the inertial sensor will be affected. However, as the IMU operating time grows and the inertial sensor temperature gradually increases, the input power required by the IMU changes, causing a change in the output voltage in the MCRWPT system. Accordingly, the MCRWPT system reflects the following characteristics from the circuit principle in supplying power to the rotating unit of the RMINS.

- (1) The coupling coefficient k is increased. Shielding the wireless power supply coil with soft magnetic material will increase the mutual inductance coupling coefficient k . Theoretical analysis shows that with the increase of k , the efficiency of the MCRWPT system will increase, but the output power may decrease.
- (2) A variable load resistance exists in the MCRWPT system. The input power required by the IMU from startup to normal operation is different. With the increase in the working time of the RMINS, the temperature change will also affect the system's input power. This paper equates the change in input power to the change in load resistance since the input voltage is constant. Variable load resistance affects the output voltage and PTE.

A simple design method for the MCRWPT system will be given in this paper, integrated with the above two points. This method focuses on the following two core issues in designing an MCRWPT system for an RMINS: (1) According to the structural characteristics of the RMINS system, the magnetic shielding structure of the wireless power supply coil is designed, and the magnetic leakage is analyzed. (2) The excitation frequency is designed to reduce the impact of load resistance changes on output voltage and PTE.

3. Design Method of MCRWPT System Based on Simulation

This paper designs the system from two main aspects of winding structure and circuit design method and applies WPT technology to an RMINS. Aiming at the internal structure of the RMINS system, this paper studies the influence of the shape of the magnetic shielding structure on the leakage magnetic field. A simple design method is proposed to match the

winding structure with the circuit, ensuring that the MCRWPT system can supply power to the IMU stably.

3.1. Ferrite Shielding Structure Design

Because there are electronic circuits, sensors, and other structures on the RMINS, which are easily affected by electromagnetic fields, it is necessary to introduce the ferrite structure to reduce the magnetic leakage of the system. In this paper, the magnetic shielding structure made of manganese-zinc ferrite is applied to reduce the influence of magnetic leakage caused by the MCRWPT system on the internal environment of the RMINS. The introduction of the magnetic shield structure changes the inductance of the primary winding and the secondary winding. Compared with the MCRWPT system with coil only, the self-inductance and mutual inductance of the MCRWPT system cannot be calculated by existing formulas [27]. Therefore, the self-inductance and mutual inductance of the system are determined by simulation.

Four ferrite structures are simulated in ANSYS Maxwell two-dimensional (2D) software to study the magnetic flux leakage characteristics of different magnetic shielding structures. Geometries of 2D simulation models are shown in Figure 5, and the dimensions of simulation models are shown in Table 2.

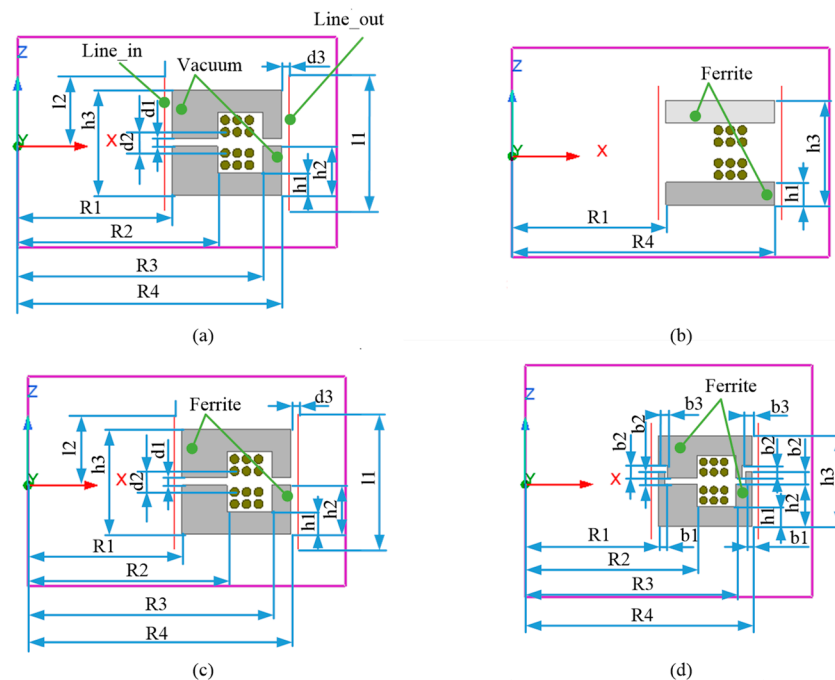


Figure 5. The geometry of the 2D simulation model. (a) Case1: without ferrite shielding. (b) Case2: with ring ferrite shielding. (c) Case3: with improved pot core ferrite shielding. (d) Case4: with special-shaped ferrite shielding.

Table 2. Dimensions of the simulation model.

Parameters	D (mm)	Parameters	D (mm)	Parameters	D (mm)
R1	20.5	h2	6.5	b1	1
R2	26.5	h3	14	b2	1.5
R3	32.5	d1	1	b3	1.5
R4	35	d2	2.8	l1	18
h1	3	d3	1	l2	9.5

The Geometry of the 2D simulation model is symmetric about the Z-axis, and Figure 5 shows only half of the 2D simulation model. The position and dimensions of coils, line-in, and line-out are all the same in Figure 5a–d. The primary and secondary coils have the same

structure, and the distance between the coils is fixed. The wire diameter of the primary coil is 1.2 mm. The coil diameter of the primary coil is 29.5 mm, and the number of turns is 6. The secondary coil is the same as the primary coil.

The 2D simulation model of winding structure for MCRWPT is constructed in ANSYS Maxwell, and the circuit is constructed in ANSYS Simpler to realize co-simulation with ANSYS Maxwell. Excitation frequency of 100 kHz, output power of 15 W, and equivalent load resistance of 100Ω are the common parameters of the simulation. Under the condition that the aforementioned common parameters are determined, the magnetic shielding performance of four different winding structures is compared through simulation. Figure 6 illustrates the magnetic flux density distributions on the XZ plane, which shows half of the magnetic flux density distribution and the other half symmetrical about the z-axis. The maximum limits of the color maps in Figure 6 are identically defined as 12 mT so that the differences in the magnetic flux density distribution between the maps can be compared. The magnetic field distribution shown in Figure 6a shows that the magnetic flux density near the coil is strong. From Figure 6b,c, it can be seen that there are obvious differences in the magnetic field distribution. Due to the directing of the magnetic field by the improved pot core ferrite shielding, the magnetic flux density inside and outside the ferrite structure is significantly reduced. Figure 6d shows the special-shaped ferrite shielding structure to reduce magnetic leakage further.

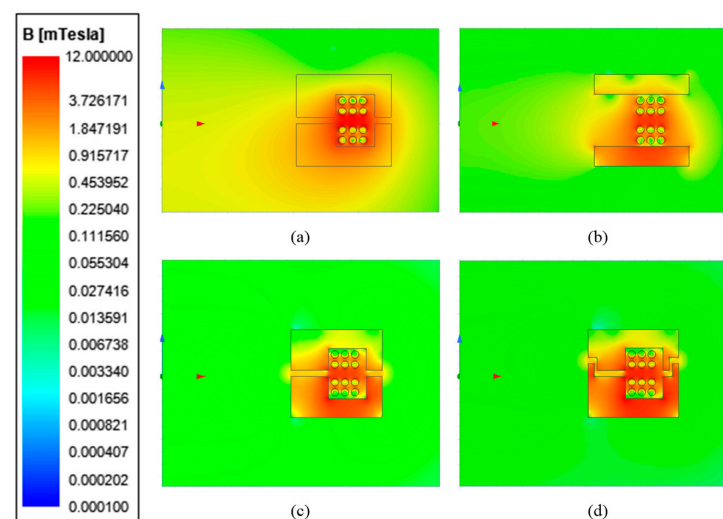


Figure 6. Magnetic field distributions on the XZ plane were simulated under the condition of constant load power. (a) Case1: without ferrite shielding. (b) Case2: with ring ferrite shielding. (c) Case3: with improved pot core ferrite shielding. (d) Case4: with special-shaped ferrite shielding.

Parameters of coils and PTE via simulation are shown in Table 3. The coil structure with ferrite shielding has a higher PTE than the coil structure without ferrite shielding. The coupling coefficient and PTE from Case1 to Case4 are gradually improved under the same output power, the same coil, and different magnetic shield structures. The special-shaped ferrite shielding, Case4, has the largest coupling coefficient and PTE.

Table 3. Parameters of coils and PTE via simulation.

Parameters [Unit]	Case1	Case2	Case3	Case4
R_1 [Ω]	78.482	103.08	166.83	166.66
R_2 [Ω]	78.49	103.08	166.81	166.06
L_1 [μH]	3.6578	6.4077	25.198	35.233
L_2 [μH]	3.6578	6.4077	25.198	35.221
k	0.68872	0.7877	0.92608	0.94713
PTE [%]	13.7	32.7	86.2	92.6

It can be seen from Figure 6 that after the introduction of the magnetic shielding structure, the magnetic induction intensity under the winding structure is smaller than the magnetic induction intensity of the side of the coil with a gap. Although the inertial sensor is installed under the winding structure, circuit components are inside the winding structure, as shown in the prototype of the uniaxial rotation module in Section 4. Therefore, the configuration of two red measuring lines located 1 mm on both sides of the ferrite shielding structure with a length of 18 mm is shown in Figure 5.

The two maximum magnitudes of the B field simulated along two red measurement lines are shown in Figure 7 to compare the magnetic flux density differences numerically. Taking the Line-in measurement line as an example, the magnetic flux density on the measurement line increases first and then decreases from bottom to top. Analysis of Figure 6 shows a maximum magnetic flux density value near the gap between the primary and secondary windings. The maximum value of the magnetic flux density obtained by the simulation based on Case1 is 1154.1 μT , while the maximum value of the magnetic flux density obtained based on Case4 is 309.5 μT . The maximum magnetic flux density on the Line-in and Line-out measurement lines decreases gradually from Case1 to Case4, as shown in Figure 7. The smaller the maximum magnetic flux density on the measurement line, the better the magnetic shielding performance of the corresponding winding structure under the condition of the same output power.

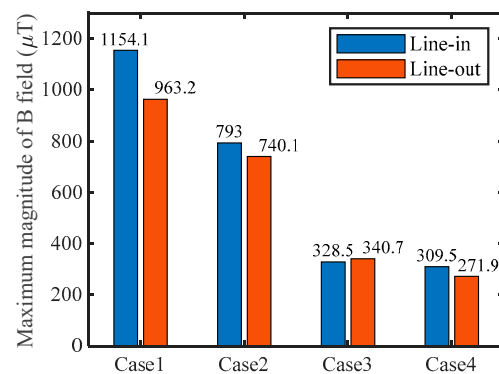


Figure 7. Magnetic flux density (maximum value) simulated under the condition of constant load power along red measurement lines.

Compared with the magnetic shielding structures of Case1 and Case2, the performance of the magnetic shielding structures of Case3 and Case4 is better, and the maximum magnitudes of the B field are close. Moreover, the magnetic shielding performance of Case4 with the special-shaped ferrite shielding is better than that of Case3 for the same distance between two windings. Compared with Case1, the magnetic leakage of Case4 decreased by 76.44%.

Case4 has the best magnetic shielding performance, the highest efficiency, and the largest coupling coefficient under the condition with the same output power. The following will take Case4 as an example for designing circuit and excitation frequency.

3.2. Design Circuit and Excitation Frequency

3.2.1. Design Circuit

In practical applications, the load resistance changes during the operation of the RMINS, resulting in a change in voltage gain. When the input voltage is fixed, the output voltage will vary and cannot provide a constant voltage for the IMU. A common method to stabilize the output voltage is to use a DC-DC boost-buck converter to adjust the output voltage of the MCRPWT system to a fixed value, such as 5 V, to power the load [21]. Therefore, the output voltage of MCRWPT needs to be properly designed to ensure that the voltage is within the input voltage range of the DC-DC converter under the condition of fixed input voltage. In addition, the introduction of a DC-DC converter reduces the total

transmission efficiency (TTE) of the power supply system, where the TTE is the product of the MCRWPT system’s efficiency and the DC-DC converter’s efficiency. Therefore, the optimization of TTE is also a problem to be solved in this paper.

The block diagram of the MCRWPT system is demonstrated in Figure 8. The transmitting circuit and receiving circuit form an MCRWPT circuit. The transmitting circuit comprises DC power U_{IN} , a full-bridge inverter circuit, primary compensation capacitors, and a primary winding. The receiving circuit consists of a secondary winding, secondary compensation capacitors, a full-wave rectifier, a filter circuit, and equivalent load resistance. R_L represents the equivalent load resistance here, including a DC-DC converter and load. The primary compensation capacitor is connected in series with the primary winding, and the secondary circuit has the same structure as the primary circuit. The DC-DC converter stabilizes the output voltage and reduces the ripple of the output voltage supplied to the load, which is the IMU. Here, V_{WPT} represents the output voltage of the MCRWPT system, and V_{OUT} represents the load voltage output by the DC-DC converter.

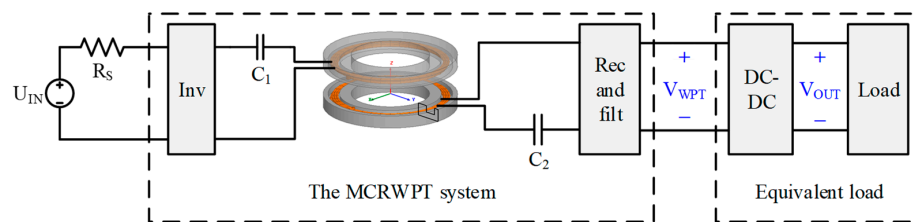


Figure 8. Block diagram of the MCRWPT system.

For the buck DC-DC converter, the symbols V_{WPT} , I_{WPT} , and R_{WPT} are defined here as the input voltage, input current, and equivalent input resistance of the DC-DC converter, respectively. Symbols V_{OUT} , I_{OUT} , and R_{OUT} are the output voltage, output current, and output load resistance, respectively. When the output power of the DC-DC converter is equal to its input power, the following formula exists.

$$V_{WPT}I_{WPT} = V_{OUT}I_{OUT} \tag{10}$$

The following relationship exists between a DC-DC converter’s the equivalent input resistance R_{WPT} and output resistance R_{OUT} .

$$R_{WPT} = \left(\frac{V_{WPT}}{V_{OUT}} \right)^2 R_{OUT} \tag{11}$$

By analyzing Equation (11), it can be known that the change of the load resistance R_{OUT} will affect the equivalent load resistance R_L of the MCRWPT system, where R_L is R_{WPT} .

3.2.2. Design Excitation Frequency

By analyzing Equations (6) and (8), the voltage gain and PTE of the MCRWPT system are affected by the coil winding, mutual inductance, equivalent load resistance, and excitation frequency. Changing the excitation frequency is a relatively simple way to adjust the output voltage and PTE, given the shape of the coil windings and the distance between the two coil windings. The TTE decreases due to the application of the DC-DC converter, so it is necessary to study the influence of excitation frequency on TTE and further optimize the TTE of the system. Designing the excitation frequency is divided into three steps: (1) Determine the excitation frequency range. (2) Excitation frequency for maximum TTE obtained without considering output power. (3) The PTE is optimized by changing the excitation frequency under the same output power condition.

The first step is to determine the excitation frequency range and ensure that the output voltage of the MCRWPT system is within the input voltage range of the DC-DC converter. Based on the model of Case4, the influence of excitation frequency on the output voltage

of the MCRWPT system is analyzed. The equivalent load resistance is assumed to vary from $10\ \Omega$ to $1\ \text{M}\Omega$. Figure 9 shows the output voltage variation with excitation frequency for different R_L . The orange curve shows that the equivalent load resistance is $1\ \text{M}\Omega$, and the output voltage increases first and then decreases with the increase of the excitation frequency. The maximum output voltage occurs at the resonant frequency of $100\ \text{kHz}$. Assuming that the input voltage is $19\ \text{V}$ and the maximum input voltage of the DC-DC converter is $40\ \text{V}$, the output voltage should be less than $40\ \text{V}$. Therefore, the design range of excitation frequency is less than $83\ \text{kHz}$, or more than $135\ \text{kHz}$. The output voltage should be more than $5\ \text{V}$, and the corresponding excitation frequency should be greater than $47\ \text{kHz}$, considering the limits of the minimum input voltage of the DC-DC converter. Because the inverter excitation frequency is limited, the maximum excitation frequency should be less than $300\ \text{kHz}$. The output voltage with R_L of $10\ \Omega$ is shown in the blue curve, and the maximum value of the output voltage is less than $40\ \text{V}$, so the output voltage is too high to damage the DC-DC converter is not considered. Therefore, the design range of excitation frequency is from $47\ \text{kHz}$ to $83\ \text{kHz}$, and from $135\ \text{kHz}$ to $300\ \text{kHz}$.

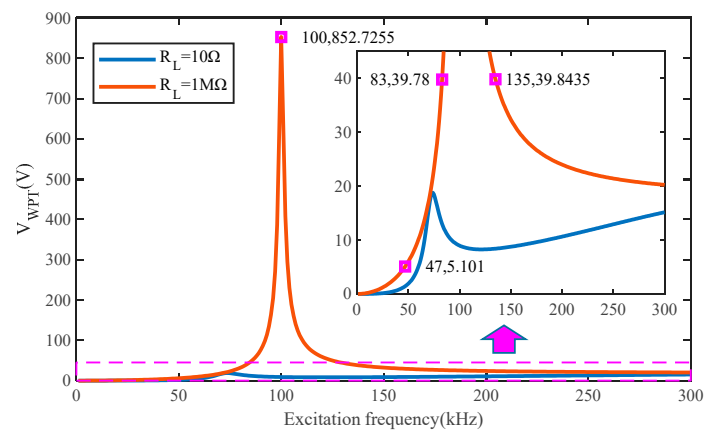


Figure 9. With different R_L , output voltage changes with excitation frequency.

The second step is to determine the excitation frequency corresponding to the maximum TTE by analyzing the influence of excitation frequency on the TTE based on the Case4 model. The resonance frequency of the MCRWPT system is $100\ \text{kHz}$, and the equivalent load resistance is fixed at $50\ \Omega$. For the same output voltage, the higher the excitation frequency, the higher the PTE, as shown in Figure 10. Therefore, the case where the excitation frequency is greater than the resonant frequency is analyzed below.

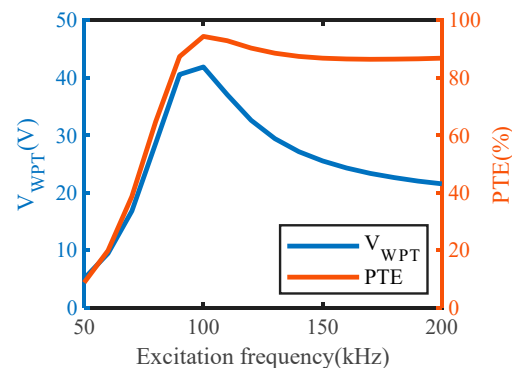


Figure 10. The output voltage and PTE vary with the excitation frequency.

As shown in the dash-dot line PTE_{WPT} in Figure 11a, the variation of PTE_{WPT} with output voltage is obtained through the joint simulation of ANSYS Maxwell and ANSYS Simplorer. When the output voltage of the DC-DC converter is fixed, the efficiency of the DC-DC converter decreases with the increase of input voltage, as shown in the dotted

line PTE_{DC} in Figure 11a. As the output voltage increases, the TTE of the system first decreases and then increases, as shown by the solid line in Figure 11a. The minimum value of TTE is 74.54%, which corresponds to an output voltage of 27.17 V and an excitation frequency of 140 kHz as shown in Figure 11a,b. The TTE can be optimized by adjusting the excitation frequency. By increasing the excitation frequency, the transmission efficiency can be increased to 76.15%, corresponding to an output voltage of 21.57 V. The excitation frequency can be obtained based on the output voltage, as shown in Figure 11b. Decreasing the excitation frequency so that the excitation frequency is close to the resonant frequency, the TTE still increases to some extent. However, it is important to ensure that the excitation frequency is within the range calculated in the first step.

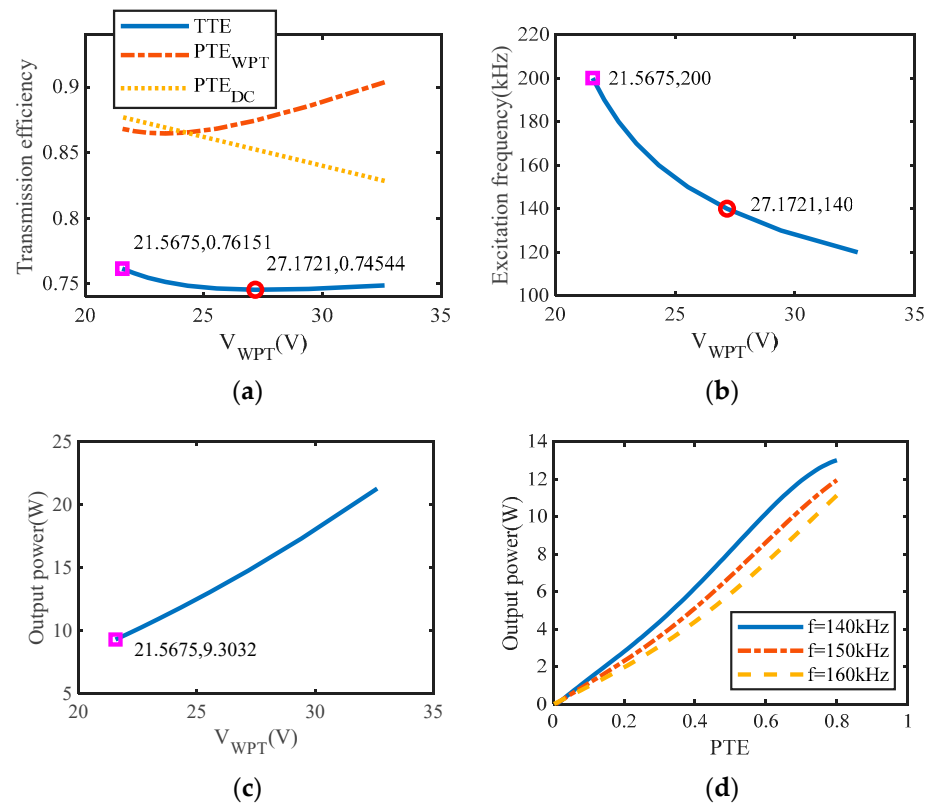


Figure 11. (a) Transmission efficiency changes with output voltage; (b) Excitation frequency changes with output voltage; (c) Output power (maximum) changes with the output voltage; (d) With different R_L , output power changes with PTE.

As shown in Figure 11c, the TTE reaches its maximum when the output voltage is 21.57 V, and the output power of the MCRWPT system reaches a minimum of less than 10 W. The output power is positively correlated with the output voltage, and the excitation frequency is negatively correlated with the output voltage. Therefore, the output power can be improved by reducing the excitation frequency, but the TTE decreases.

The last step is to optimize the TTE by changing the excitation frequency under the same output power condition. The TTE is the product of the MCRWPT system’s efficiency and the DC-DC converter’s efficiency. The efficiency of a DC-DC converter increases as the difference between the input voltage and the output voltage decreases. Figure 11a,b shows that as the excitation frequency increases, the output voltage decreases, and the efficiency of the DC-DC converter increases. The relationship between efficiency and output power is obtained under different excitation frequencies, as shown in Figure 11d. Under the same output power condition, the higher the excitation frequency, the higher the PTE. Compared with the other two excitation frequencies, the output efficiency is the highest when the excitation frequency is 160 kHz. Therefore, optimizing TTE is to increase the excitation frequency of the system under the condition of guaranteeing the output power.

4. Experiment

An experimental platform was implemented to verify the effectiveness of the theory and simulation, as shown in Figure 12. The experimental platform comprises a DC power supply, a wireless power transmitter PCB, a transmitter coil with ferrite, a receiver coil with ferrite, a wireless power receiver PCB, load resistance, and an acrylic plate with 1 mm thickness. The magnetic shielding performance of Case3 and Case4 is similar, with a fixed distance between primary and secondary windings. It can be seen from Table 3 that the coupling coefficient of Case3 is smaller than that of Case4. Therefore, the MCRWPT system based on Case3 has a higher output power capability under the same gap, and the structure of Case3 is simple and easy to process. Hence, the experimental winding structure is the same as Case3. Litz wire was used to form the two coils. The transmitting coil has six turns of Litz wire made with 105 strands of American-wire-gauge 40, and the receiving coil is the same as the transmitting coil. The coil parameters measured by the precision LCR digital bridge TH2838H are shown in Table 4. Compared with the simulation results of Case3 in Table 3, there are errors in the coil parameters tested in the experiment, which may be caused by inaccurate simulation modeling. However, it does not affect the analysis of system characteristics through simulation.

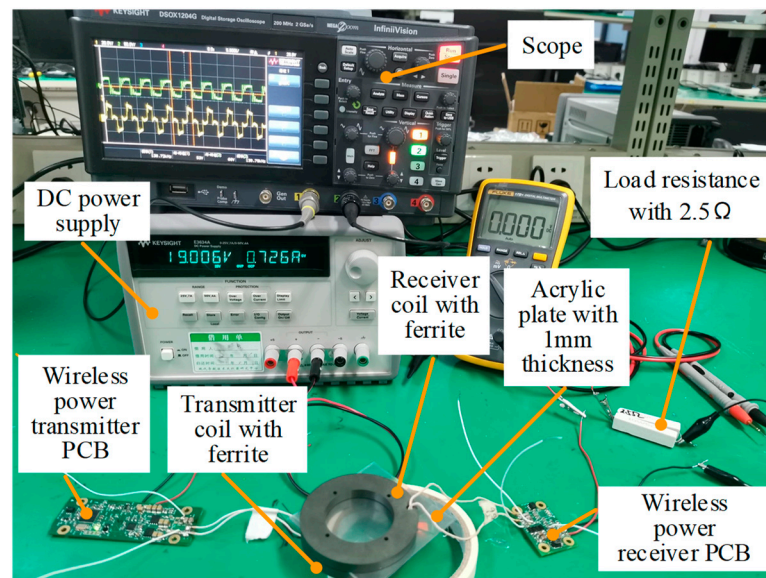


Figure 12. Experimental prototype of an MCRWPT system.

Table 4. Parameters of coils via experiment.

Parameters [Unit]	Case3
R_1 [Ω]	0.25
R_2 [Ω]	0.28
L_1 [μH]	28.109
L_2 [μH]	28.328
k	0.8258

The main circuit components and parameters used in the experimental prototype are shown in Figure 13. The TS61002 is a high-voltage full-bridge driver used to drive N-channel devices. Furthermore, the input voltage U_{IN} is 19 V. The internal resistance R_S of the power supply is related to the inverter and its pre-circuit and is considered a small value in this experiment. A DC-DC converter, TS30042, was used to maintain an input voltage of 5.0 V to the load resistance. TS30042 has a maximum output power of 10 W. The load resistance was designed to be 2.5 Ω to test the designed system with an output power of 10 W. The specific configuration of the inverter and DC-DC converter's peripheral circuits

can be referred to in their data sheets. In order to reduce the electromagnetic interference generated by the DC-DC converter, refer to the TS30042 data sheet for the PCB layout of the DC-DC converter and peripheral components.

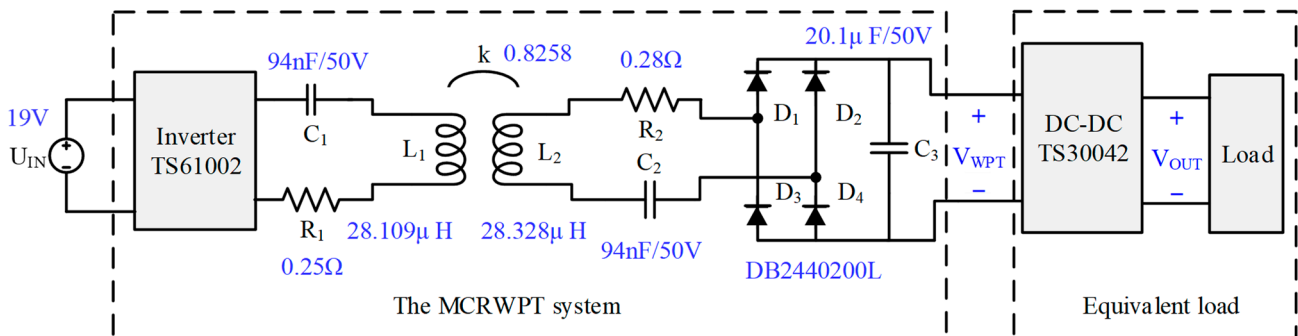


Figure 13. The main circuit components and parameters used in the experimental prototype.

The experimental prototype of the MCRWPT system is applied to the uniaxial rotation module inertial navigation system (URMINS) designed by our laboratory. The URMINS consists of three same uniaxial rotation modules and one navigation and power management module. The rotation axes of the three uniaxial rotation modules are perpendicular to each other and form a Cartesian coordinate system. Each module transmits the demodulated specific forces and angular rates to the CAN bus’s navigation and power management module. The navigation and power management module furnishes the vehicle’s current position, velocity, and attitude.

Figure 14 shows that the MCRWPT system is applied to a uniaxial rotation module prototype. The motor drives the rotating unit to rotate continuously in the uniaxial rotation module at a low speed. The load on the rotating unit mainly consists of two single-axis fiber optic gyroscopes, two single-axis quartz flexible accelerometers, wireless communication PCB 1#, and an information processing unit. The power required by the load does not exceed 10 W, the voltage is 5 V, and the startup and normal operating currents are within 2 A, so the experimental prototype of the MCRWPT system can supply power to the uniaxial rotation module. Wireless communication and MCRWPT technologies are adopted in the uniaxial rotation module to avoid cable winding and wear of slip ring. The MCRWPT system powers the load on the rotating unit, and the data of the inertial sensors (gyroscopes and accelerometers) is output to the upper computer through wireless communication.

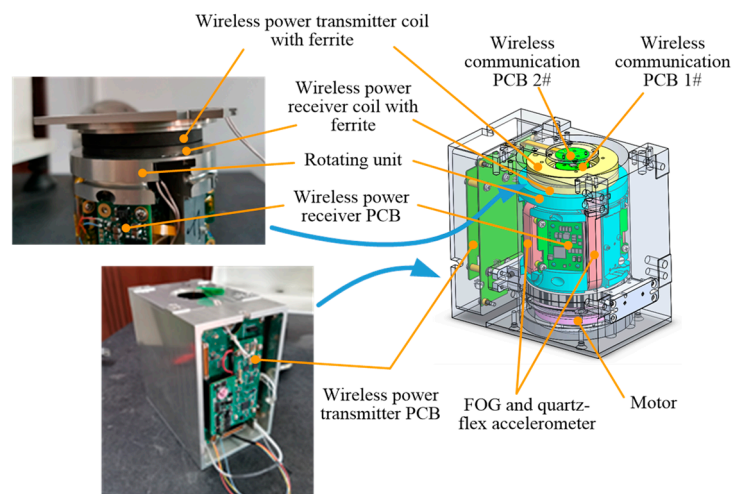


Figure 14. The prototype of the uniaxial rotation module used the MCRWPT system.

The maximum input voltage of the DC-DC converter used in the experiment is 40 V, and the output voltage is 5 V, so the ratio of V_{WPT}/V_{OUT} cannot exceed 8. When the

load resistance R_{OUT} is 2.5Ω , the equivalent load resistance R_L is 160Ω , calculated by Equation (11). When the output power is reduced to 1.6 mW , the load resistance is $15.625 \text{ k}\Omega$, and the equivalent load resistance is $1 \text{ M}\Omega$. When the load power is more than 1.6 mW and the output voltage is 5 V , the excitation frequency working range of the system can be obtained through the excitation frequency design method in Section 3.2.2. Considering that when the input voltage of the DC-DC converter is about 22.4 V , the output power is 10 W , and the equivalent load resistance of the system is calculated by Equation (11) to be 50Ω . It is reasonable to choose 50Ω as equivalent load resistance in circuit design to analyze the characteristics of the circuit.

System characteristic parameters include output voltage, output power, and TTE, and their relationship with excitation frequency is shown in Figure 15a. When the excitation frequency is 138.7 kHz , 143.35 kHz , and 145.3 kHz , the effective value of output power is 10 W , the output voltage of the MCRWPT system decreases, and the TTE increases gradually. The effectiveness of simulation analysis is verified.

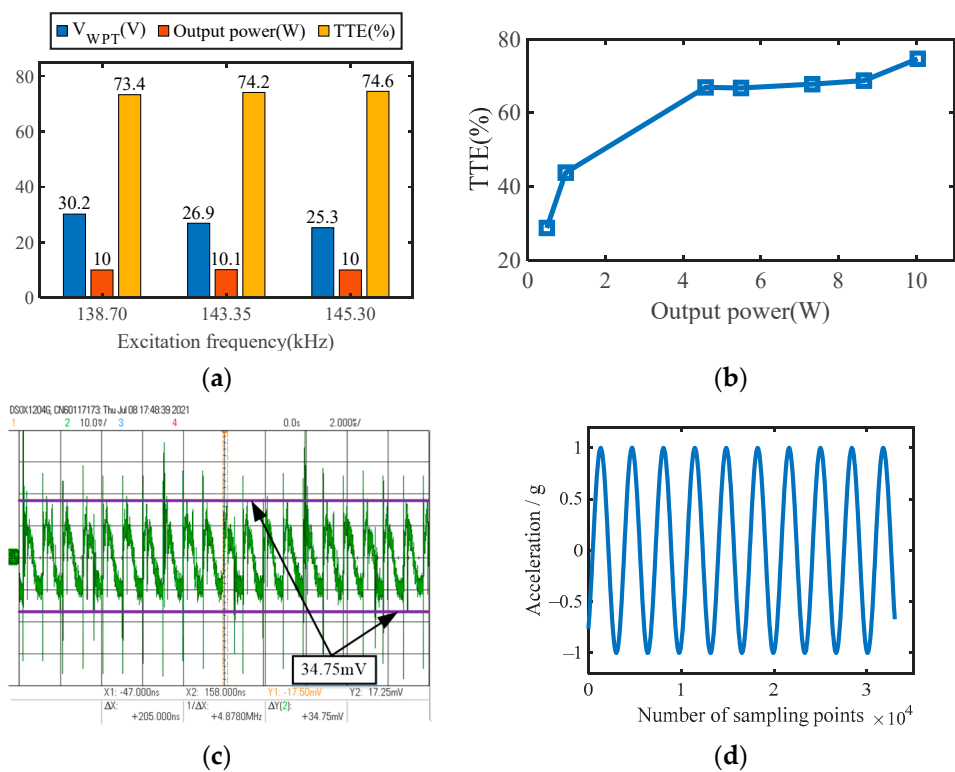


Figure 15. (a) System characteristic parameters at different excitation frequencies measured by experiment; (b) The relationship between TTE and output power under $f = 145.3 \text{ kHz}$; (c) The ripple of output load voltage; (d) An accelerometer’s measurement with the motor continuously rotating.

The excitation frequency is 145.3 kHz , and the output load voltage is 5 V . The output power varies with the load resistance. Furthermore, the TTE decreases with the decrease of output power, and the results are shown in Figure 15b, which is consistent with the simulation analysis. The output voltage ripple measured with an oscilloscope is shown in Figure 15c. The output voltage ripple is 34.75 mV , which is less than 50 mV , which meets the requirements of the inertial sensor for the supply voltage. Figure 15d shows the accelerometer data when the rotating unit rotates at a constant speed in the uniaxial rotation module.

Experiments prove that the proposed MCRWPT method can be successfully applied to a uniaxial rotation module of a URMINs. At the same time, the effectiveness of the proposed design method is proved. The TTE of the MCRWPT systems is 74.6% at the output power of 10 W . The advantage of the approach in this article is that it is simple to

implement and does not require any feedback. The shortcoming of this paper is that the PTE of the MCRWPT system gradually decreases with the decrease of the output power.

5. Conclusions

This paper applied the WPT technology to the RMINS, solving the problems of wire tangling and frictional wear of slip-rings and providing a stable power supply to the IMU. According to the characteristics of the RMINS, a simple design method of the MCRWPT system based on SS compensation topology was given. Specifically, the magnetic shielding structure's magnetic leakage characteristics and SS compensation topology system characteristics were analyzed based on ANSYS software. The DC-DC converter was adopted to stabilize the output voltage of the secondary side with the varying load resistance. The influence of excitation frequency on system efficiency was analyzed, and the TTE was optimized by increasing excitation frequency. The experimental results showed that the designed MCRWPT system can achieve a TTE of 74.6% at an output power of 10 W and can successfully power inertial sensors and PCBs on the rotating unit of the uniaxial rotation module in the URMINS. The experimental results verify the effectiveness of the proposed method, which can simplify the design process of the WPT system and have guiding significance for engineering practice.

Author Contributions: Conceptualization, M.N. and X.S.; methodology, M.N. and K.S.; software, H.M.; validation, M.N. and Z.Z.; formal analysis, T.H.; investigation, Z.Z.; writing—original draft preparation, M.N.; writing—review and editing, X.S. and T.H. All authors have read and agreed to the published version of the manuscript.

Funding: This research received no external funding.

Institutional Review Board Statement: Not applicable.

Informed Consent Statement: Not applicable.

Data Availability Statement: The data that support the findings of this study are available from the corresponding author upon reasonable request.

Conflicts of Interest: The authors declare no conflict of interest.

References

1. Kang, L.; Ye, L.; Song, K.; Zhou, Y. Attitude Heading Reference System Using MEMS Inertial Sensors with Dual-Axis Rotation. *Sensors* **2014**, *14*, 18075–18095. [[CrossRef](#)] [[PubMed](#)]
2. Chen, G.; Li, K.; Wang, W.; Li, P. A Novel Redundant INS Based on Triple Rotary Inertial Measurement Units. *Meas. Sci. Technol.* **2016**, *27*, 105102. [[CrossRef](#)]
3. Levinson, E.; Majure, R. Accuracy Enhancement Techniques Applied to the Marine Ring Laser Inertial Navigator (MARLIN). *Navigation* **1987**, *34*, 71–80. [[CrossRef](#)]
4. Legranger, J.; Friedrich, G.; Vivier, S.; Mipo, J.C. Comparison of Two Optimal Rotary Transformer Designs for Highly Constrained Applications. In Proceedings of the 2007 IEEE International Electric Machines Drives Conference, Antalya, Turkey, 3–5 May 2007; Volume 2, pp. 1546–1551.
5. Jia, J.; Yan, X. Application of Magnetic Coupling Resonant Wireless Power Supply in a Torque Online Telemetry System of a Rolling Mill. *J. Electr. Comput. Eng.* **2020**, *2020*, e8582131. [[CrossRef](#)]
6. Zhang, Y.; Zhou, B.; Song, M.; Hou, B.; Xing, H.; Zhang, R. A Novel MEMS Gyro North Finder Design Based on the Rotation Modulation Technique. *Sensors* **2017**, *17*, 973. [[CrossRef](#)]
7. Wu, C.; Kim, H.; Penugonda, S.; Fan, J. Analysis and Modeling of the Common-Mode Conducted EMI from a Wireless Power Transfer System for Mobile Applications. *IEEE Trans. Electromagn. Compat.* **2021**, *63*, 2143–2150. [[CrossRef](#)]
8. Cai, Q.; Yang, G.; Song, N.; Yin, H.; Liu, Y. Analysis and Calibration of the Gyro Bias Caused by Geomagnetic Field in a Dual-Axis Rotational Inertial Navigation System. *Meas. Sci. Technol.* **2016**, *27*, 105001. [[CrossRef](#)]
9. Wang, L.; Lu, Y.; Xu, Y.; Yang, Z.; Zhao, L. Error Characteristics of Magnetic Field in Depolarized Interferometric Fiber Optic Gyroscope. *Opt. Eng.* **2010**, *49*, 064402. [[CrossRef](#)]
10. Liao, Y.-H.; Lin, Y. A Novel Bidirectional Wireless Power Transfer System for Mobile Power Application. *Appl. Sci.* **2019**, *9*, 3769. [[CrossRef](#)]
11. Zhang, Y.; Zhao, Z.; Chen, K. Frequency Decrease Analysis of Resonant Wireless Power Transfer. *IEEE Trans. Power Electron.* **2014**, *29*, 1058–1063. [[CrossRef](#)]

12. Han, G.; Liu, Y.; Guo, S.; Han, T.; Li, Q. Design of Coaxial Coupled Structure for Distance-Insensitive Wireless Power Transfer. *Rev. Sci. Instrum.* **2019**, *90*, 074708. [[CrossRef](#)] [[PubMed](#)]
13. Wang, X.; Pang, J.; Tan, Q.; Dong, H.; Zhao, N.; Xue, T. Design of Double-Layer Parallel Printed Spiral Coil for Wireless Power Transfer Applied to Rotating Equipment. *Sens. Actuators A Phys.* **2021**, *331*, 112761. [[CrossRef](#)]
14. Patil, D.; McDonough, M.K.; Miller, J.M.; Fahimi, B.; Balsara, P.T. Wireless Power Transfer for Vehicular Applications: Overview and Challenges. *IEEE Trans. Transp. Electrification*. **2018**, *4*, 3–37. [[CrossRef](#)]
15. Kim, J.; Kim, J.; Kong, S.; Kim, H.; Suh, I.-S.; Suh, N.P.; Cho, D.-H.; Kim, J.; Ahn, S. Coil Design and Shielding Methods for a Magnetic Resonant Wireless Power Transfer System. *Proc. IEEE* **2013**, *101*, 1332–1342. [[CrossRef](#)]
16. Kim, H.; Song, C.; Kim, J.; Jung, D.H.; Song, E.; Kim, S.; Kim, J. Design of Magnetic Shielding for Reduction of Magnetic near Field from Wireless Power Transfer System for Electric Vehicle. In Proceedings of the 2014 International Symposium on Electromagnetic Compatibility, Gothenburg, Sweden, 1–4 September 2014; pp. 53–58.
17. Smeets, J.P.C.; Krop, D.C.J.; Jansen, J.W.; Hendrix, M.A.M.; Lomonova, E.A. Optimal Design of a Pot Core Rotating Transformer. In Proceedings of the 2010 IEEE Energy Conversion Congress and Exposition, Atlanta, GA, USA, 12–16 September 2010; pp. 4390–4397.
18. Bastiaens, K.; Krop, D.C.J.; Jumayev, S.; Lomonova, E.A. Optimal Design and Comparison of High-Frequency Resonant and Non-Resonant Rotary Transformers. *Energies* **2020**, *13*, 929. [[CrossRef](#)]
19. Sohn, Y.H.; Choi, B.H.; Lee, E.S.; Lim, G.C.; Cho, G.-H.; Rim, C.T. General Unified Analyses of Two-Capacitor Inductive Power Transfer Systems: Equivalence of Current-Source SS and SP Compensations. *IEEE Trans. Power Electron.* **2015**, *30*, 6030–6045. [[CrossRef](#)]
20. Hui, S.Y.R.; Zhong, W.; Lee, C.K. A Critical Review of Recent Progress in Mid-Range Wireless Power Transfer. *IEEE Trans. Power Electron.* **2014**, *29*, 4500–4511. [[CrossRef](#)]
21. Plaizier, G.M.; Andersen, E.; Truong, B.; He, X.; Roundy, S.; Leang, K.K. Design, Modeling, and Analysis of Inductive Resonant Coupling Wireless Power Transfer for Micro Aerial Vehicles (MAVs). In Proceedings of the 2018 IEEE International Conference on Robotics and Automation (ICRA), Brisbane, Australia, 21–25 May 2018; pp. 6104–6109.
22. Vinko, D.; Pavlović, I.; Runac, K. Application of DC-DC Converters in Loosely Coupled Wireless Power Transmission Systems. In Proceedings of the 2017 International Conference on Smart Systems and Technologies (SST), Osijek, Croatia, 18–20 October 2017; pp. 51–54.
23. Li, H.; Li, J.; Wang, K.; Chen, W.; Yang, X. A Maximum Efficiency Point Tracking Control Scheme for Wireless Power Transfer Systems Using Magnetic Resonant Coupling. *IEEE Trans. Power Electron.* **2015**, *30*, 3998–4008. [[CrossRef](#)]
24. Yin, J.; Lin, D.; Lee, C.K.; Hui, S.Y.R. Load Monitoring and Output Power Control of a Wireless Power Transfer System without Any Wireless Communication Feedback. In Proceedings of the 2013 IEEE Energy Conversion Congress and Exposition, Denver, CO, USA, 15–19 September 2013; pp. 4934–4939.
25. Zhong, W.X.; Hui, S.Y.R. Maximum Energy Efficiency Tracking for Wireless Power Transfer Systems. *IEEE Trans. Power Electron.* **2015**, *30*, 4025–4034. [[CrossRef](#)]
26. Kiani, M.; Ghovanloo, M. The Circuit Theory Behind Coupled-Mode Magnetic Resonance-Based Wireless Power Transmission. *IEEE Trans. Circuits Syst. I Regul. Pap.* **2012**, *59*, 2065–2074. [[CrossRef](#)]
27. Dai, Z.; Wang, J.; Li, Y.; He, Y.; Fang, Z.; Hou, H. Optimal Design of Magnetic Coupling Wireless Power Supply System for Monitoring Equipment. *IEEE Access* **2018**, *6*, 58600–58608. [[CrossRef](#)]